Thermochimica Acta 500 (2010) 13–20

Contents lists available at ScienceDirect

Thermochimica Acta

journal homepage: www.elsevier.com/locate/tca

Non-isothermal crystallization kinetics of polyamide-6/graphite oxide nanocomposites

Yan Liu [a], Guisheng Yang [a,b,*]

[a] Department of Polymer Science and Engineering, Zhejiang University, Hangzhou, Zhejiang 310027, PR China
[b] Shanghai Genius Advanced Materials Co., Ltd, Shanghai 201109, PR China

ARTICLE INFO

Article history:
Received 28 August 2009
Received in revised form 1 December 2009
Accepted 7 December 2009
Available online 14 December 2009

Keywords:
Graphite oxide
Polyamide-6
Kinetics
Non-isothermal crystallization
Nanocomposites

ABSTRACT

Polyamide-6 (PA6)/graphite oxide (GO) nanocomposite was synthesized using delamination/absorption with dimethylacetamide as solvent. TEM showed that graphite oxide sheets were completely exfoliated and distributed uniformly in polyamide-6 matrix. Non-isothermal crystallization behaviors of PA6 and nanocomposites were investigated using DSC. The modified Avrami, Mo and Ozawa equation were employed to investigate the crystallization process. The former two could successfully describe the non-isothermal crystallization of PA6 and nanocomposites. It was interesting to find that Ozawa equation could successfully describe the non-isothermal crystallization of nanocomposites, but it was not valid for PA6. The crystallization rate of nanocomposites greatly decreased by the addition of GO, which confirmed by the results of half-time of crystallization ($t_{1/2}$), crystallization rate exponent Z_c and $\log F(T)$. Also, the more the content of GO, the slower the crystallization rate. The effective activation energy calculated from Friedman formula suggested that the layered structure of GO restrained the crystallization of PA6.

1. Introduction

Polyamide-6 (PA6) is an important group of the thermoplastic with excellent solvent resistance and good processability. However, PA6 exhibits a relatively rapid crystallization rate, which makes it to have some drawbacks such as high mold shrinkage and dimensional instability. In order to control the crystallization rate and the crystallinity, then achieve the desired morphology and properties, a great deal of efforts has been made on studying the crystallization kinetics corresponding to the change of the performed properties [1–5].

During the last decades, nanocomposites generate a great deal of interest from materials scientists because of their potentially novel properties. Their merit is such that they can be transformed into new materials possessing the advantages of both organic materials, such as light-weight, flexibility, good moldability and inorganic materials, such as high strength, heat stability and chemical resistance. The incorporation of organic/inorganic hybrids can result in materials possessing excellent of stiffness, strength and gas barrier properties [6]. Various inorganic particles, such as montmorillonite, $CaCO_3$, SiO_2, $BaSO_4$, are usually used as filler in the polymer matrix. Among these fillers, montmorillonite has been given particular attention due to its inherent layered structure [7–10].

Graphite oxide (GO), also has the layered structure as montmorillonite, has attracted interest in the scientific community, especially in recent years [11–14]. GO is hydrophilic and has been shown to undergo intercalation chemistry with polar macromolecular such as polyethylene oxide [15], poly(vinyl alcohol) [16,17] and poly(ε-caprolactone) [18]. Moreover, less polar polymers such as poly(styrene) [19] have also been successfully incorporated into the gallery space of graphite oxide. These composites not only uniformly disperse in matrix, but also possess improved mechanical and thermal properties without phase separation.

In this work, PA6/GO nanocomposites were prepared using delamination/absorption with dimethylacetamide (DMAC) as solvent. The morphology was investigated by transmission electronic microscopy (TEM). The non-isothermal crystallization kinetics for nanocomposites, as compared with those for pure PA6, was investigated using differential scanning calorimetry (DSC). The experimental data was analyzed based on the commonly used modified Avrami equation, Ozawa theory and Mo formula, respectively. The effective activation energy for non-isothermal crystallization process of different samples was calculated by Friedman equation.

2. Experimental

2.1. Materials

PA6 used in this study was a product of Ube Industries. Expandable graphite was supplied by Shandong New Fangyuan Industry Co., Ltd., P.R. China. Graphite oxide was prepared from expansible

* Corresponding author at: Shanghai Genius Advanced Materials Co., Ltd, Shanghai 201109, PR China. Tel.: +86 21 64881869; fax: +86 21 64907216.
E-mail address: ygs@geniuscn.com (G. Yang).

0040-6031/$ – see front matter © 2010 Elsevier B.V. All rights reserved.
doi:10.1016/j.tca.2009.12.003

graphite by the modified Hummers method [20] and dried at 60 °C for 24 h in a vacuum oven.

2.2. Fabrication of PA6/GO nanocomposites

PA6/GO composite was synthesized by delamination/absorption. 0.5 g GO was immersed in 100 ml DMAC and sonicated for 30 min to form delaminated suspension. The PA6 solution was prepared by dissolve 2.0 g PA6 in 100 ml DMAC. The GO suspension was transferred quickly into DMAC solution of PA6 with drastically stirring. Then the obtained mixture was poured into the beaker, filtered and washed with acetone to remove DMAC. The resulting PA6/GO composite was dried at 60 °C for 24 h in a vacuum oven before characterization. Pristine PA6 was treated under the same procedure as for nanocomposites without adding GO. Corresponding to weight percentage of GO, the composites were designated as PA6-0 (0% GO), PA6-5 (5% GO), PA6-10 (10% GO).

2.3. Characterization

Transmission electronic microscopy (TEM) was carried out on a Hitachi H-800 microscope at an acceleration voltage of 100 kV. The samples were ultramicrotomed with a diamond knife on a Leica Ultracut UCT microtomed at room temperature to give nanometer thick sections.

The non-isothermal crystallization and subsequent melting behavior of all the samples were studied by the PerkinElmer Diamond DSC instrument (Shelton, CT). Temperature calibration was carried out using an indium standard ($T_m^0 = 156.6\,^{\circ}C$ and

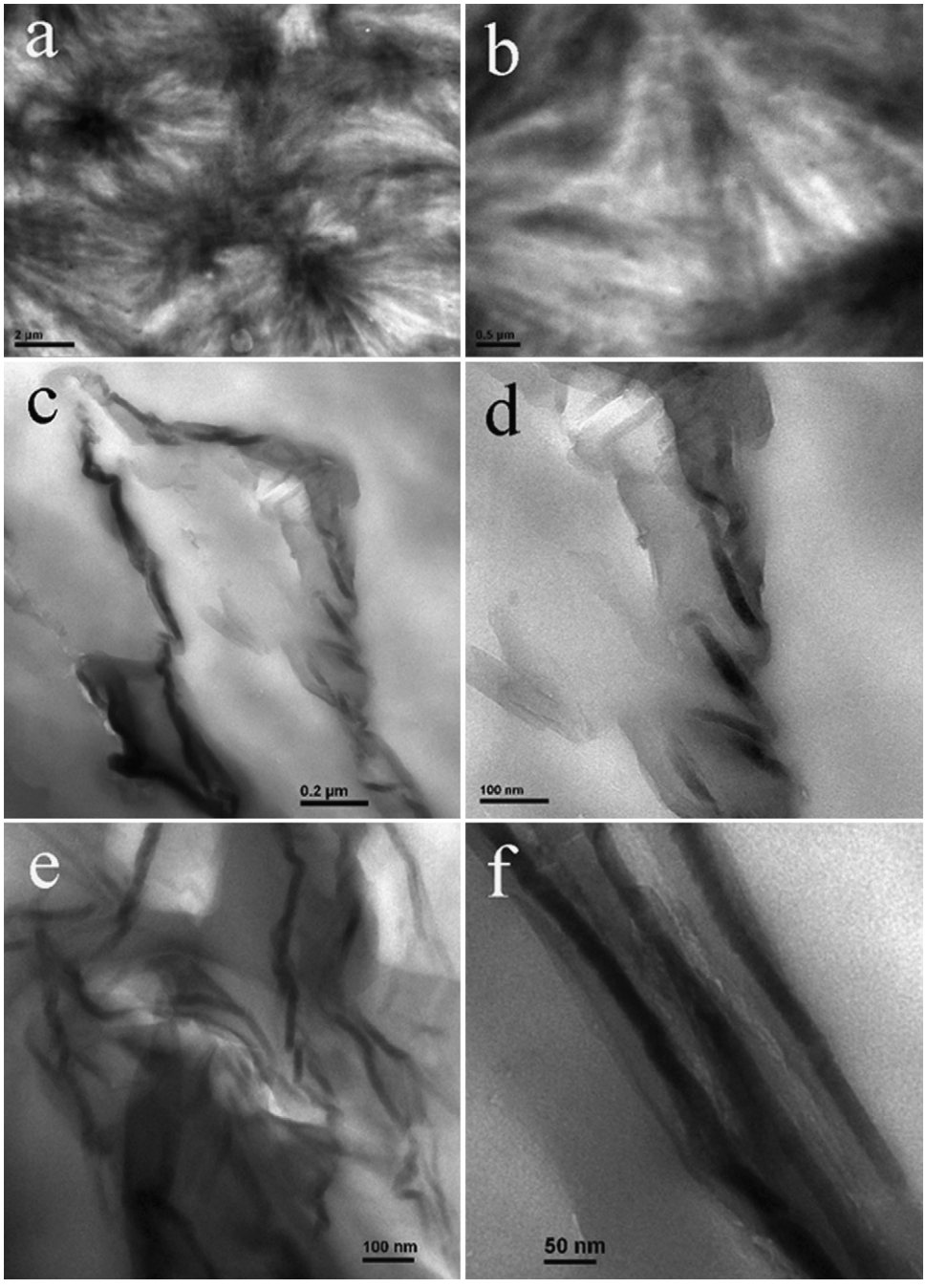

Fig. 1. TEM images of PA6 (a and b), PA6-5 (c and d) and PA6-10 (e and f) with different magnifications.

$\Delta H_f^0 = 28.5\,J\,g^{-1}$). The consistency of the temperature calibration was checked every other run to ensure the reliability of the data obtained. To avoid an uneven thermal conduction of the samples, which may cause different amounts of broadening and shifting of the peak positions, the aluminum pans were always filled with the same quantity of specimen, about 6.0 ± 0.2 mg. The samples were heated at a rate of 60 °C/min from room temperature to 260 °C under nitrogen atmosphere and held for 5 min to remove the thermal history. The non-isothermal crystallization kinetics was investigated by cooling these samples to 50 °C at the rate of 5, 10, 20, 30 and 40 °C/min, respectively. The subsequent melting behavior of each sample was recorded immediately at a heating rate of 20 °C/min. The heat of crystallization ΔH_c is normalized by the GO weight percent.

3. Results and discussion

3.1. TEM observation

Fig. 1 shows the TEM images of PA6 (a and b), PA6-5 (c and d) and PA6-10 (e and f) with different magnifications. For pure PA6 (Fig. 1a and b), the morphology is typical spherulites which are formed of fibrils that are more densely packed in the center. For the nanocomposites (Fig. 1c–f), most of the GO sheets (disordered dark lines), with a layer thickness of 10–20 nm, dispersed well in PA6 matrix, which proves that the GO are exfoliated and randomly and homogeneously dispersed on the molecular level. In addition, large aspect ratio has been found in GO sheets (Fig. 1f). The fine dispersion and large aspect ratio of the GO sheets in the composite inevitable effect the crystallization behavior as discussed next.

3.2. Non-isothermal crystallization and subsequent melting behavior

The relative crystallinity (X_t) as a function of temperature is defined as the following equation:

$$X_t = \frac{\int_{t_0}^{t}(dH/dt)dt}{\int_{t_0}^{t_\infty}(dH/dt)dt} \quad (1)$$

where t_0 and t_∞ are the time, at which crystallization starts and ends, respectively.

The crystallization time t can be obtained by the following equation:

$$t = \frac{|T_s - T|}{\varphi} \quad (2)$$

where T is the temperature at a crystallization time t, T_s is the temperature at which crystallization starts and φ is the cooling rate.

The non-isothermal crystallization exothermic peaks of PA6-0 and PA6-10 at various cooling rate are shown in Fig. 2 and the kinetic parameters are summarized in Table 1. It is found that when the cooling rate is increased, the peak crystallization temperature T_p shifts to lower temperatures and the crystallization exotherm becomes wider for all the samples. In detail, the T_ps decrease from 195.6 to 180.3 °C for pure PA6 and from 199.9 to 186.7 °C for PA6-10 with increasing cooling rates, which is attributed to the low time scale that allows the polymer to crystallize with increasing cooling rate. Thus, a higher super-cooling to initiate crystallization is required, and the exotherms become broader.

As seen in Table 1, the values of T_p of PA6-5 and PA6-10 shift to high temperature compared with neat PA6 at a given cooling rate, which indicates that the GO can increase the melt-crystallization temperature. The crystallization enthalpies (ΔH_c) decrease gradually for all samples with increasing cooling rates. When the specimens are cooled fast, the motion of the molecular chain is not able to follow the cooling temperature, and then the molecular chains become less mobile and have short time to diffuse into the crystallite lattice; thus, they can only adjust and organize the chain conformation into less perfect crystallites [21]. Furthermore, the ΔH_c of PA6/GO composites are higher than that of neat PA6 at

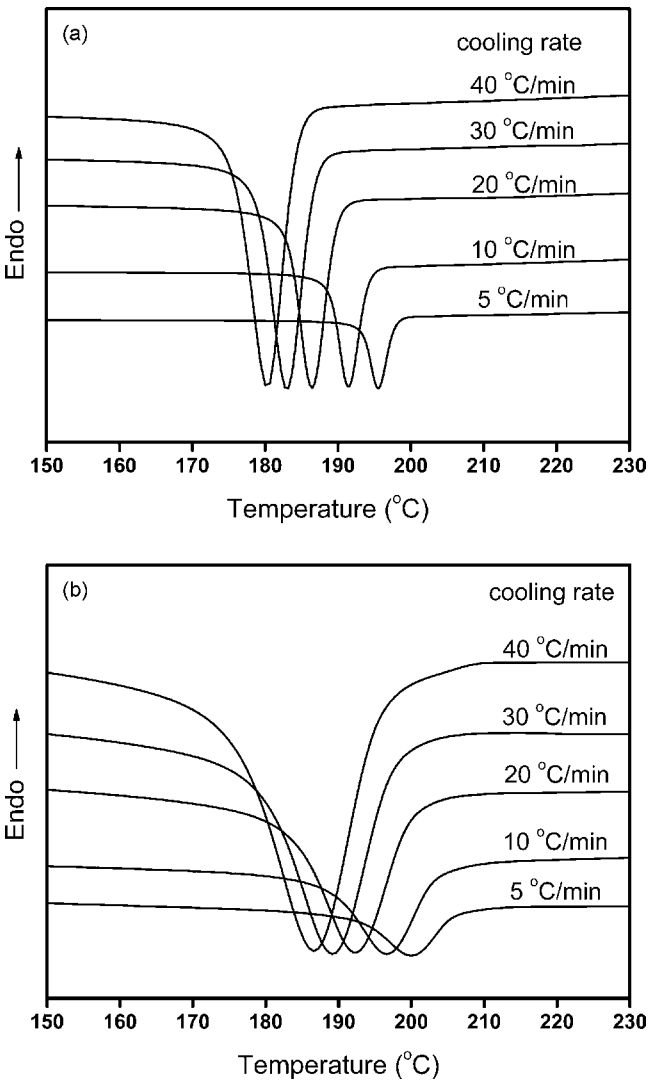

Fig. 2. Non-isothermal melt-crystallization exotherm of (a) PA6 and (b) PA6/GO nanocomposite at different cooling rates.

Table 1
Kinetic parameters of non-isothermal crystallization for various samples.

Samples	φ (°C/min)	T_p (°C)	$t_{1/2}$ (s)	ΔH_c (J/g)	n	Z_c
PA6-0	5	195.6	61.1	−54.8	5.02	0.17
	10	191.5	33.8	−52.7	4.84	0.48
	20	186.6	22.0	−50.6	4.86	0.72
	30	183.0	15.6	−47.0	4.71	0.83
	40	180.3	13.2	−42.2	4.56	0.87
PA6-5	5	198.0	101.3	−56.5	4.64	0.15
	10	194.5	55.7	−54.7	4.52	0.43
	20	189.9	36.0	−54.0	4.59	0.70
	30	185.9	25.1	−46.8	4.27	0.79
	40	184.2	22.9	−43.9	4.09	0.86
PA6-10	5	199.9	142.7	−59.7	4.58	0.14
	10	196.7	82.9	−58.1	4.34	0.42
	20	192.3	52.2	−56.4	4.23	0.67
	30	189.2	36.1	−50.1	4.18	0.78
	40	186.7	34.0	−45.6	4.12	0.80

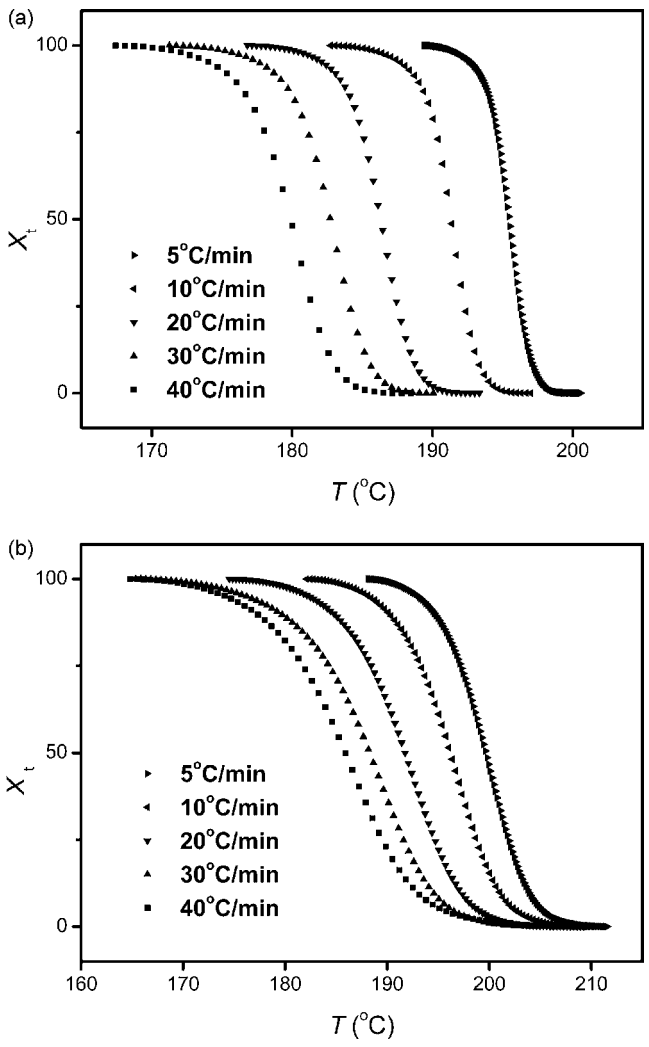

Fig. 3. Relative crystallinity vs. temperature for non-isothermal crystallization of (a) PA6-0 and (b) PA6-10 nanocomposites at different cooling rates.

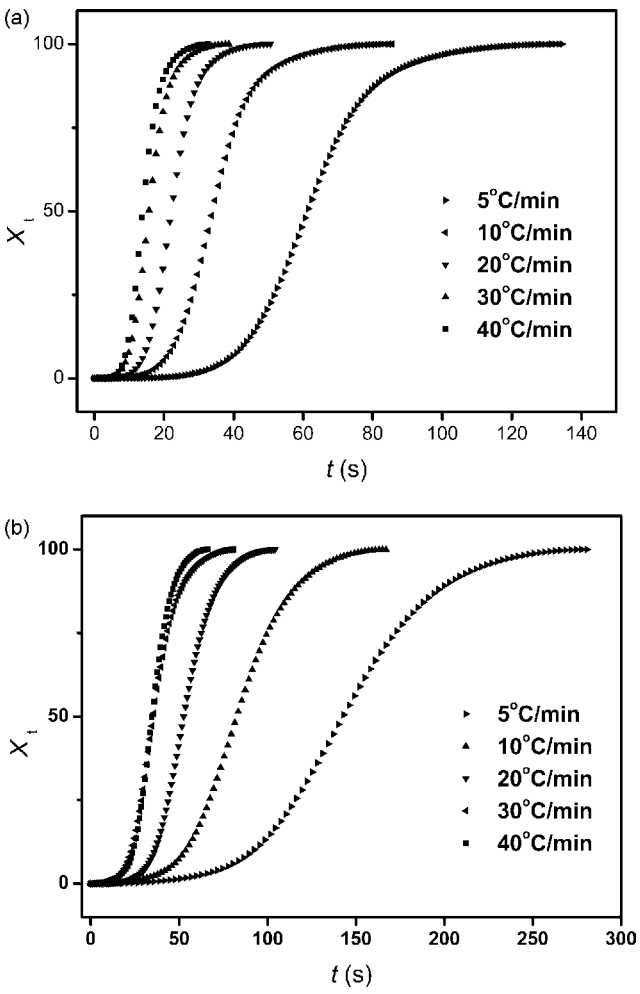

Fig. 4. Relative crystallinity vs. time for non-isothermal crystallization of (a) PA6-0 and (b) PA6-10 nanocomposites at different cooling rates.

a given cooling rate, suggesting that the total crystallinity of the nanocomposites are promoted by GO. Possible reason is that GO increases the crystallization temperature, which results in a longer crystallization time.

From DSC crystallization curves of PA6-0 and PA6-10, the relative crystallinity as a function of temperature at different cooling rates is shown in Fig. 3(a) and (b). It can be seen that all these curves have similar sigmoidal shape, with a fast primary crystallization during the early stage and a slow secondary crystallization at the later stage. The curvature of the upper part plot is observed to level off which already begin from the inflection point of the curves due to the spherulites impingement or crowding in the final stage of crystallization. The data can be further analyzed by converting the temperature scale of the $X_c(T)$ function into the time scale using Eq. (2), to obtain the relative crystallinity function of time $X_c(t)$. The converted curves are illustrated in Fig. 4(a) and (b). It can be seen that all these curves shift to left via t-axial with increasing cooling rates, indicating a lower scale of crystallization time or faster crystallization rate with increasing cooling rates.

Another important parameter is the half-time of crystallization ($t_{1/2}$), which is defined as the time taken from the onset of $X_c(t)$ until 50% completion. The dependence of $t_{1/2}$ on cooling rate (φ) for various samples is listed in Table 1. With increasing φ, $t_{1/2}$ decreases accordingly both for pure PA6 and the composites, this indicates that the samples can crystallize more quickly at higher cooling rate. At a given φ, $t_{1/2}$ of the composites is evidently longer than that of pure PA6, and this suggests an apparent decrease in the crystallization rate when GO is loaded into the polymer matrix. Moreover, the more the content of GO, the slower the crystallization rate (for the reasons, see the last paragraph of the next section).

The subsequent melting thermograms for PA6-0 and PA6-10 after non-isothermal crystallization process are shown in Fig. 5(a) and (b), and the melting endotherm parameters are summarized in Table 2. As seen in Fig. 5, double melting endotherms are observed at high cooling rates (i.e., >10 °C/min) for PA6. These endotherms are labeled as peaks I and II for high- and low-temperature melting endotherms, respectively. Peaks II shifts to lower temperature as the cooling rate increases and peak I changes little. However, remarkable differences can be found for the nanocomposites, i.e., only one melting endotherm (T_{mI}) is observed, also, T_{mI} decreases somewhat with increasing cooling rate. Peaks I and II ascribed to the melting peaks of the α-crystalline form [22–24] and γ-crystalline form [22–25], respectively [26]. For pure PA6, the α-crystalline is predominant at low cooling rate whereas the γ-crystalline form gradually strengthens with increasing cooling rate. On the contrary, for the nanocomposites, the γ-crystalline form is absent. Moreover, the heat of melting (ΔH_m) of the nanocomposites is lower than that of neat PA6 at lower GO content and higher at higher GO content, as seen in Table 2.

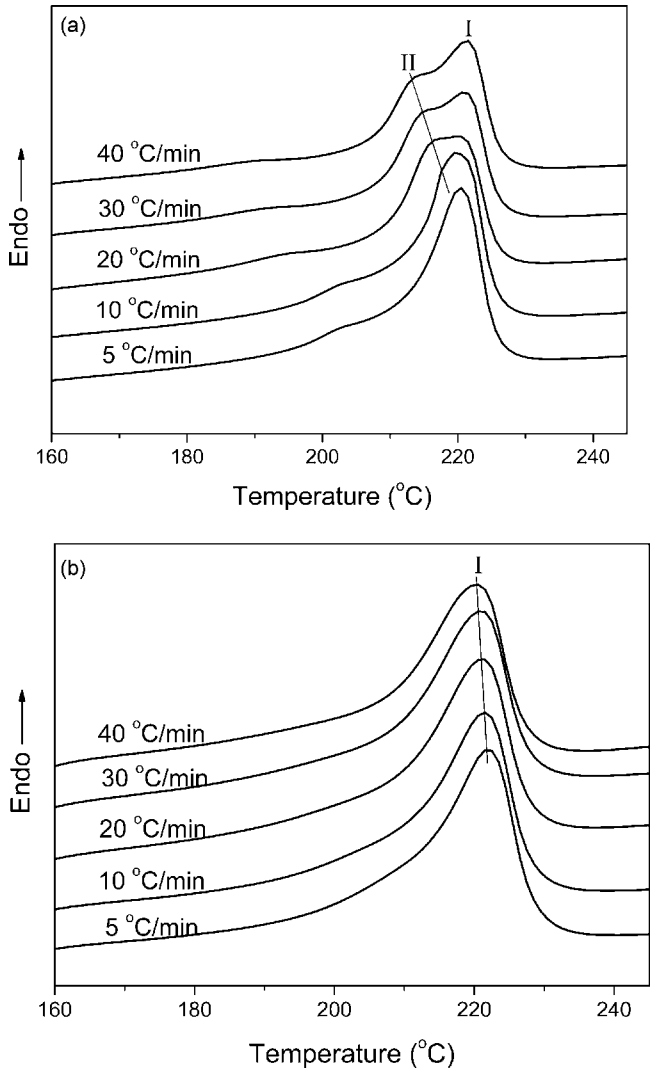

Fig. 5. Subsequent melting endotherms of (a) PA6-0 and (b) PA6-10 recorded at a heating rate of 20 °C/min after non-isothermal crystallization.

3.3. Non-isothermal crystallization kinetics analysis

3.3.1. Analysis based on the Avrami theory modified by Jeziorny

Assuming that the crystallization temperature remained constant when the cooling rate was kept constant [27,28], the modified Avrami equation can be used to analyze the non-isothermal crystallization process of PA6 and the nanocomposites. It can be illuminated in the following form:

$$1 - X_c = \exp(-Z_t t^n) \tag{3}$$

$$\log[-\ln(1 - X_c)] = n \log t + \log Z_t \tag{4}$$

The exponent n is a mechanism constant with a value depending on the type of nucleation and the growth dimension, and the parameter Z_t is a growth rate constant involving both nucleation and growth rate parameters. Jeziorny [29] considered the values of Z_t determined by Avrami equation should be corrected as follows:

$$\log Z_c = \frac{\log Z_t}{|\varphi|} \tag{5}$$

where Z_c is the kinetic crystallization rate constant.

Fig. 6(a) and (b) shows a series of double logarithm plot of $\log[-\ln(1 - X_t)]$ vs. $\log t$ at different cooling rates. All curves are divided into the following two sections: the primary crystallization stage and the secondary crystallization stage. The Avrami exponent n and Z_t are obtained from the slopes and the intercepts, respectively. They are listed in Table 1. The Avrami exponent n are found to range from 4.6 to 5.0 for PA6, from 4.1 to 4.6 for the composites when cooling rates increased from 5 to 40 °C/min. The values of n decreased gradually with increasing cooling rate for each sample, indicating the crystallization growth is on fewer dimensions with increasing cooling rate. At the primary stage,

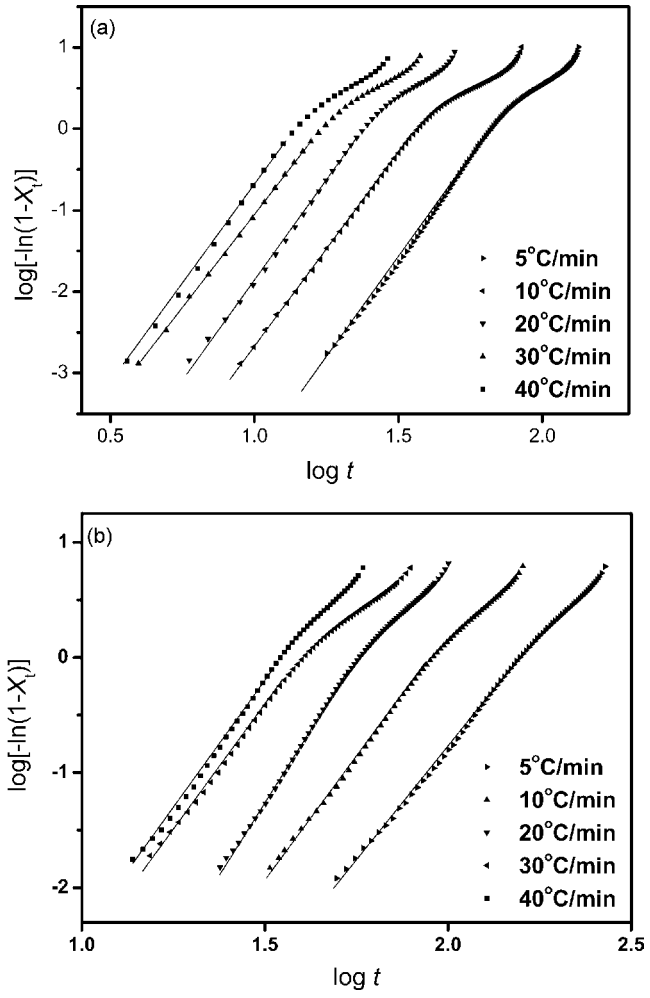

Fig. 6. Plots of $\log[-\ln(1 - X_c)]$ vs. $\log t$ for non-isothermal crystallization of (a) PA6-0 and (b) PA6-10 nanocomposites.

Table 2
Subsequent melting endotherm parameters of various samples.

Samples	φ (°C/min)	T_{mI} (°C)	T_{mII} (°C)	ΔH_m (J/g)
PA6-0	5	220.3	–	52.0
	10	220.0	217.7	51.2
	20	220.7	216.2	51.3
	30	221.0	214.9	48.2
	40	221.3	213.3	43.4
PA6-5	5	221.5	–	52.6
	10	221.0	–	48.9
	20	220.6	–	49.9
	30	220.3	–	45.3
	40	220.0	–	40.7
PA6-10	5	222.0	–	55.8
	10	221.3	–	52.9
	20	221.1	–	52.1
	30	220.9	–	44.9
	40	220.3	–	40.0

the Avrami exponent, n is 4.8 ± 0.2, indicates a thermal nucleation and a three-dimensional spherical growth mechanism [30]. However, for the nanocomposites, n is 4.8 ± 0.2. Its nucleation type should mostly be a heterogeneous nucleation and its crystal growth dimension should mostly be three-dimensional space extension.

As shown in Table 1, another overall rate parameter, Z_c, determines both the nucleating and growth processes, which are extremely sensitive to temperature for each sample. That is, the higher the temperature, the lower the crystallization rate. Comparing the Z_c of pure PA6 and the composites at a given cooling rate, we find that the latter shows a low value, which indicates a slow crystallization rate for the composites. Moreover, with increasing GO loading, Z_c decreases accordingly. In other words, the more the GO content, the lower the crystallization rate.

Actually, there are two factors controlling the crystallization rate of polymeric composite systems. One is that additives have a nucleating effect, which results in an increase in Z_c, a positive effect on crystallization. The other is that the additives hinder the migration and diffusion of polymer molecular chains to the surface of the nucleus, and they constrain spherulitic growth by an impingement mechanism in the composites, which results in decreasing Z_c, a negative effect on crystallization. In this case, the positive effect is relatively feeble and the layered structure of GO (as seen in Fig. 1) predominantly constrains the migration and diffusion of PA6 at so high GO loading (i.e., 5 and 10 wt.%) [31].

3.3.2. Analysis based on the Ozawa theory

Assuming that crystallization occurs at a constant cooling rate φ, and the crystallization originates from a distribution of nuclei that grow as spherulites with a constant radial growth rate at a given temperature, Ozawa extended the Avrami equation to the non-isothermal condition as follows:

$$1 - X_t = \exp\left[\frac{-K(T)}{\varphi^m}\right] \tag{6}$$

$$\log[-\ln(1 - X_t)] = \log\ K(T) - m \log \varphi \tag{7}$$

where m is the Ozawa exponent, and $K(T)$ is the kinetics crystallization rate constant. If we plot $\log[-\ln(1 - X_t)]$ against $\log \varphi$ at a given temperature, a linear response is obtained if the Ozawa analysis is valid, and m and $K(T)$ can be estimated accordingly.

The results of the Ozawa analysis for PA6-0 and PA6-10 are shown in Fig. 7(a) and (b), respectively. From Fig. 7(a), it is evident that the Ozawa analysis does not adequately describe the non-isothermal crystallization kinetics of PA6. Possible reason is that Ozawa assumed that the effects of secondary crystallization were negligible because it occurred in the later period and the temperature decreased in the cooling crystallization process. However, the secondary crystallization is influenced greatly by the outside factors such as fillers and cooling rate, and the effect could not be neglected for the non-isothermal crystallization of some polymer systems. Similar results have been also reported by Qu et al. [32]. It is interesting to find that the Ozawa theory is valid for PA6/GO nanocomposites and a series of straight lines are obtained. The reason for this is, for PA6/GO composites, a large amount of GO nuclei preexist in the amorphous PA6 and a thermal nucleus is absent. So the crystallization is mainly controlled by the diffusion of PA6 chains onto the growth front. However, the special structure of GO (i.e., layered, with large aspect ratio) constrains the migration and diffusion of PA6, which result in a slower crystallization rate and later secondary crystallization. In other words, the primary crystallization plays a predominant role and the second crystallization becomes less predominant [33] in PA6/GO system and these may be the reasons that Ozawa theory is valid for PA6/GO nanocomposites.

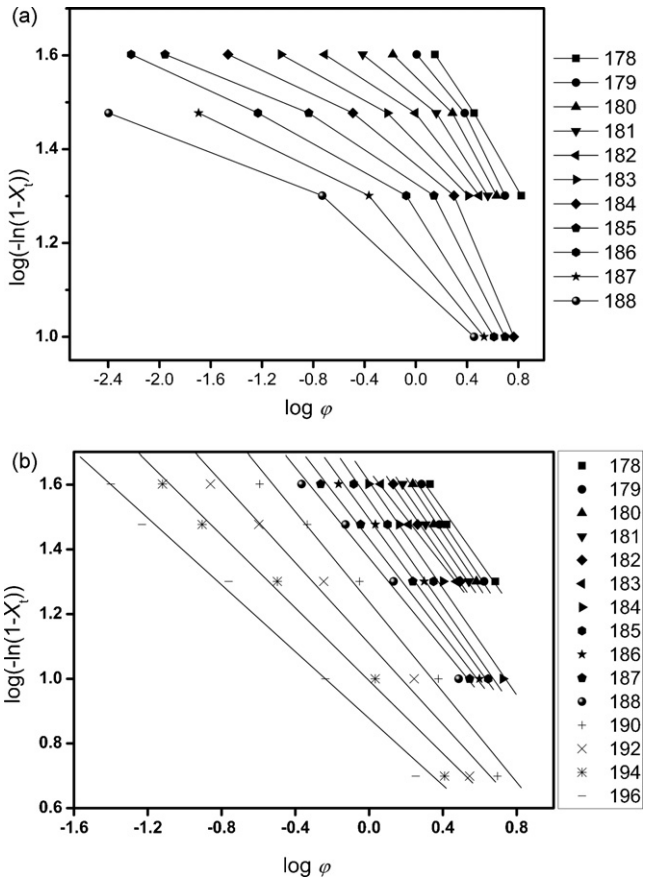

Fig. 7. Ozawa plots of $\log[-\ln(1 - X_t)]$ vs. $\log D$ for (a) PA6-0 and (b) PA6-10 nanocomposites.

3.3.3. Analysis based on the Mo theory

Mo et al. proposed a different kinetic equation by combining the Avrami and Ozawa equations [34]. As the degree of crystallinity is related to the cooling rate φ and the crystallization time t (or T), the relationship between φ and t could be defined for a given degree of crystallinity. Consequently, a new kinetic equation for non-isothermal crystallization was derived by combining Eqs. (4) and (7):

$$\log Z_t + n \log t = \log K(T) - m \log\ \varphi \tag{8}$$

$$\log \varphi = \log F(T) - b\ \log t \tag{9}$$

Let $F(T) = [K(T)/Z_t]^{1/m}$, and $b = n/m$. n is the Avrami parameter, and m is the Ozawa exponent. $F(T)$ means the value of the cooling rate, which has to be chosen at unit crystallization time when the measured system amounts to a certain degree of crystallization. $F(T)$ has a definite physical and practical meaning.

According to Mo's method, plots of $\log \varphi$ against $\log t$ at a given degree of crystallinity will give a straight line with an intercept of $\log F(T)$ and a slope of $-b$ if Mo analysis is valid. As shown in Fig. 8, plotting $\log \varphi$ against $\log t$ for PA6-0 and PA6-10 composites demonstrates linear relationship at a given X_t, and the values of $\log F(T)$ and b are listed in Table 3. The values of $\log F(T)$ are increased with the relative crystallinity from 2.00 to 3.33 (for PA6-0), 3.21 to 3.54 (for PA6-5), and 3.59 to 3.81 (for PA6-10), indicating that a lower crystallization rate is needed to reach the given degree of crystallinity within unit time. The parameter b shows only a small increase with increasing X_t, ranging from 1.37 to 1.42 (for PA6-0), 1.40 to 1.42 (for PA6-5), and 1.40 to 1.42 (for PA6-10), respectively. Compared the values of $\log F(T)$ of PA6-0 with those of PA6-5 and PA6-10 at a given X_t, it is obvious that the results of PA6-0 is smaller

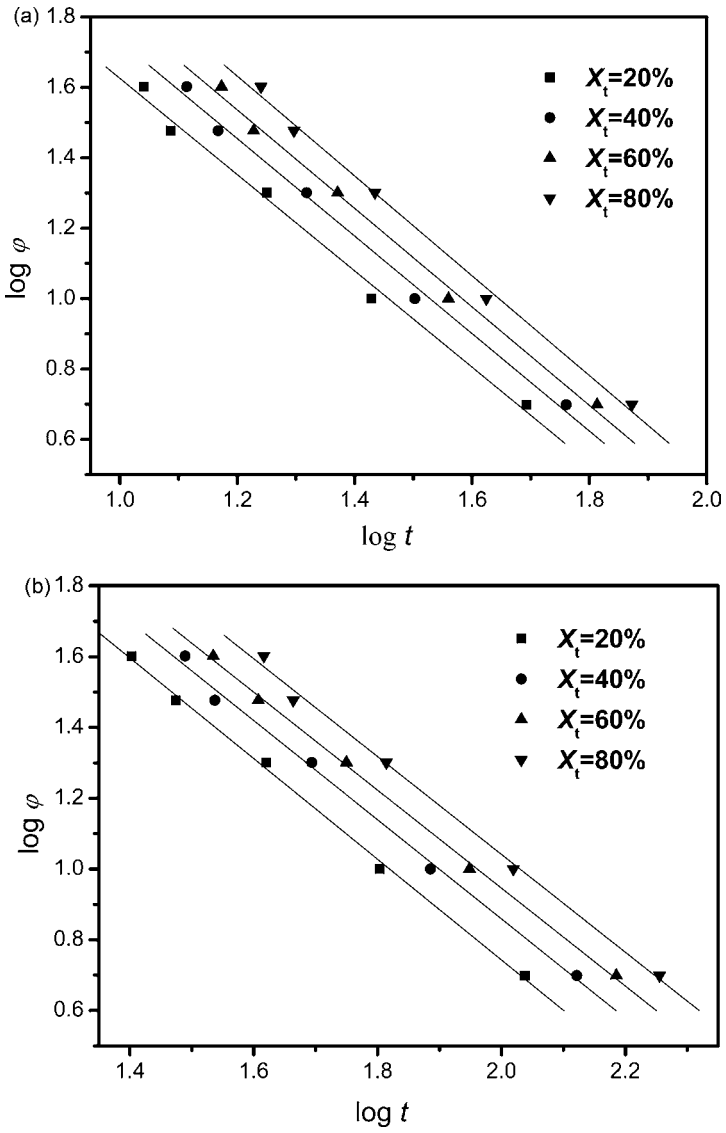

Fig. 8. log D vs. log t from the Mo equation for (a) PA6-0 and (b) PA6-10 nanocomposites.

than those of PA6-5 and PA6-10, indicating that GO decreases crystallization rate of PA6, and the more the GO content, the lower the crystallization rate. This conclusion is consistent with the analysis of Avrami. Thus, the equation of Mo method successfully describes the non-isothermal crystallization process of PA6/GO composites.

3.4. Effective activation energy

Friedman [35] and Vyazovkin [36–38] developed the differential iso-conversional method for evaluating the effective activation energy for non-isothermal crystallization process. The kinetic equation can be written as $d\alpha/dt = k(T)f(\alpha)$, where $k(T)$ is the Arrhenius constant, α is the conversion degree and $f(\alpha)$ is the function describing the reaction mechanism. The relation above described, in the logarithm form, is:

$$\ln\left(\frac{d\alpha}{dt}\right)_\alpha = \ln(A_\alpha f(\alpha)) - \frac{E_\alpha}{RT_\alpha} \quad (10)$$

where R is the universal gas constant, A_α, E_α, and T_α are the pre-exponential factor, the effective activation energy and temperature at a certain conversion degree α, respectively.

The analysis by Friedman theory for PA6-0 is shown in Fig. 9. A series of straight lines were obtained, then E_a can be derived from the slope (i.e., $\Delta E_a = (\text{slope})(R)$). The ΔE_a values determined for various values of α, ranging from 0.1 to 0.9 with 0.2 increment, are summarized in Table 4. Apparently, the ΔE_a parameter is found to increase monotonically for three samples when α is increased,

Table 3
Non-isothermal crystallization kinetic parameters of PA6-0, PA6-5 and PA6-10 analyzed by Mo equation.

X_t (%)	PA6-0		PA6-5		PA6-10	
	b	log $F(T)$	b	log $F(T)$	b	log $F(T)$
20	1.37	2.99	1.40	3.21	1.40	3.59
40	1.38	3.12	1.41	3.36	1.40	3.66
60	1.40	3.21	1.42	3.41	1.41	3.71
80	1.42	3.33	1.42	3.54	1.42	3.81

Table 4
Effective activation energy of PA6-0, PA6-5 and PA6-10.

Samples	0.1	0.3	0.5	0.7	0.9
PA6-0	−199.2	−178.9	−158.7	−148.9	−140.1
PA6-5	−182.4	−165.5	−144.3	−138.2	−116.5
PA6-10	−161.0	−132.3	−127.2	−114.6	−84.5

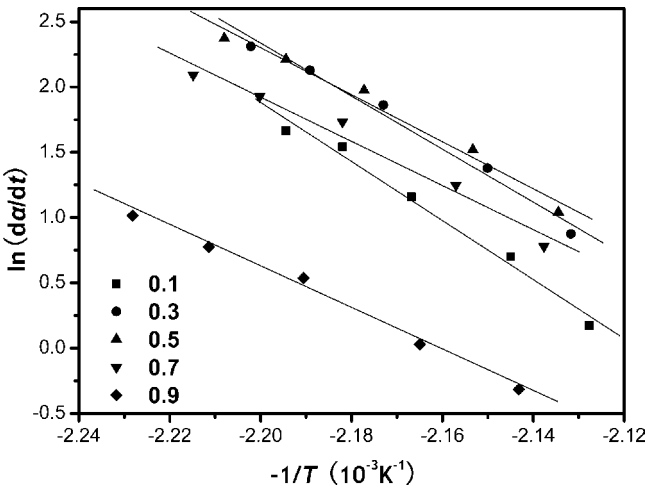

Fig. 9. Friedman plots of $\ln(d\alpha/dt)$ vs. $(-1/T)$ for PA6-0.

suggesting that, as the crystallization progressed, it is more difficult for the polymer to crystallize. Similar results have been reported in other literature [37–40]. In addition, comparing the ΔE_a values of PA6-0, PA6-5 and PA6-10 at the same α (e.g., $\alpha = 0.5$), we find that ΔE_a increases with increasing GO loading, which indicates that the nano-particles make the transportation chains of PA6 to a growing crystal surface more difficult. This result is consistent with the crystallization rate results of modified Avrami theory and Mo analysis, as mentioned previously.

4. Conclusion

Polyamide-6/graphite oxide nanocomposite was synthesized using delamination/absorption with dimethylacetamide as solvent. The morphology of the nanocomposite was characterized by TEM. It was shown that the GO sheets, with a layer thickness of 10–20 nm, dispersed well in PA6 matrix, which proved that the GO was exfoliated and homogeneously dispersed. Non-isothermal crystallization behaviors of pure PA6 and the composites were investigated by DSC. The modified Avrami equation, Mo formula and Ozawa theory were employed to investigate the crystallization process. The former two could successfully describe the non-isothermal crystallization of PA6 and nanocomposites. It was interesting to find that the Ozawa equation can successfully describe the non-isothermal crystallization of nanocomposites, but it was not valid for pure PA6. The crystallization rate of nanocomposites was greatly decreased by the addition of GO, which confirmed by the results of $t_{1/2}$, Z_c or the $\log F(T)$. Also, the more the content of GO, the slower the crystallization rate. Possible reason was that the layered structure of GO constrains the migration and diffusion of PA6. The effective activation energy calculated from Friedman formula suggested that the layered structure of GO made the molecular chains of PA6 more difficult to crystallize during the non-isothermal crystallization process.

References

[1] T. Ozawa, Polymer 12 (1971) 150–158.
[2] C.X. Zhou, S.B. Clough, Polym. Eng. Sci. 28 (1988) 65–68.
[3] X. Lu, J.N. Hay, Polymer 42 (2001) 9423–9431.
[4] B. Lee, T.J. Shin, S.W. Lee, J. Yoon, J. Kim, H.S. Youn, M. Ree, Polymer 44 (2003) 2509–2518.
[5] M.T. Run, S.Z. Wu, D.Y. Zhang, G. Wu, Polymer 46 (2005) 5308–5316.
[6] J.H. Chang, S.J. Kim, Y.L. Joo, S. Im, Polymer 45 (2004) 919–926.
[7] Y.Q. Rao, J.M. Pochan, Macromolecules 40 (2007) 290–296.
[8] M.A. Paul, C. Delcourt, M. Alexandre, P. Degée, F. Monteverde, A. Rulmont, P. Dubois, Macromol. Chem. Phys. 206 (2005) 484–498.
[9] A. Okada, A. Usuki, Macromol. Mater. Eng. 291 (2006) 1449–1476.
[10] Z.H. Tong, Y.L. Deng, Ind. Eng. Chem. Res. 45 (2006) 2641–2645.
[11] T. Cassagneau, F. Guérin, J.H. Fendler, Langmuir 16 (2000) 7318–7324.
[12] T. Cassagneau, J.H. Fendler, Adv. Mater. 10 (1998) 877–881.
[13] R. Ding, Y. Hu, Z. Gui, R. Zong, Z. Chen, W. Fan, Polym. Degrad. Stabil. 81 (2003) 473–476.
[14] N.I. Kovtyukhova, P.J. Olliver, B.R. Martin, T.E. Mallouk, S.A. Chizhik, E.V. Buzaneva, A.D. Gorchinskiy, Chem. Mater. 11 (1999) 771–778.
[15] Y. Matsuo, K. Tahara, Y. Sugie, Carbon 35 (1997) 113–120.
[16] Y. Matsuo, K. Hatase, Y. Sugie, Chem. Mater. 10 (1998) 2266–2269.
[17] J. Xu, Y. Hu, L. Song, Q. Wang, W. Fan, G. Liao, Z. Chen, Polym. Degrad. Stabil. 73 (2001) 29–31.
[18] L. Hua, W.H. Kai, Y. Inoue, J. Appl. Polym. Sci. 106 (2007) 4225–4232.
[19] M. Xiao, L. Sun, J. Liu, Y. Li, K. Gong, Polymer 43 (2002) 2245–2248.
[20] W.S. Hummers, R.E. Offeman, J. Am. Chem. Soc. 80 (1958) 1339–11339.
[21] M.T. Run, C.G. Yao, Y.J. Wang, H.Z. Song, Polym. Compos. 29 (2008) 1235–1243.
[22] L. Penel-Pierron, C. Depecker, R. Seguela, J.M. Lefebvre, J. Polym. Sci. B: Polym. Phys. 39 (2001) 484–495.
[23] Y.P. Khanna, W.P. Kuhn, J. Polym. Sci. B: Polym. Phys. 35 (1997) 2219–2231.
[24] K.H. Illers, H. Haberkorn, P. Simak, Makromol. Chem. 158 (1972) 285–311.
[25] J.P. Sibilia, N.S. Murthy, M.K. Gabriel, M.E. McDonnell, R.G. Bray, S.A. Curran, in: M.I. Kohan (Ed.), Nylon Plastics Handbook, Hanser Publishers, New York, 1995, pp. 69–106.
[26] A.D. Liu, T.X. Xie, G.S. Yang, Macromol. Rapid Commun. 27 (2006) 1572–1577.
[27] M.L. Xue, J. Sheng, Y.L. Yu, H.H. Chuah, Eur. Polym. J. 40 (2004) 811–818.
[28] L. Mandelkern, Methods of Experimental Physics, Academic Press, New York, 1980, pp. 81–105.
[29] A. Jeziorny, Polymer 19 (1978) 1142–1144.
[30] B. Wunderlich, Macromolecular Physics: Crystal Nucleation, Growth, Annealing, vol. 2, Academic Publishers, New York, 1976, pp. 69–106.
[31] C.G. Yao, T.X. Xie, G.S. Yang, J. Appl. Polym. Sci. 109 (2008) 3562–3570.
[32] X.W. Qu, H.L. Ding, J.Y. Lu, Y.X. Wang, L.C. Zhang, J. Appl. Polym. Sci. 93 (2004) 2844–2855.
[33] X.B. Hu, A.J. Lesser, Macromol. Chem. Phys. 205 (2004) 574–580.
[34] T. Liu, Z. Mo, H. Zhang, J. Appl. Polym. Sci. 67 (1998) 815–821.
[35] H.L. Friedman, J. Polym. Sci. C 6 (1964) 183–186.
[36] S. Vyazovkin, J. Comput. Chem. 18 (1997) 393–402.
[37] S. Vyazovkin, N. Sbirrazzuoli, Macromol. Rapid. Commun. 25 (2004) 733–738.
[38] S. Vyazovkin, I. Dranca, Macromol. Chem. Phys. 207 (2006) 20–25.
[39] M.T. Run, H.Z. Song, C.G. Yao, Y.J. Wang, J. Appl. Polym. Sci. 106 (2007) 868–877.
[40] A. Nattapol, S. Pitt, N. Manit, Polym. Test. 23 (2004) 817–822.